

Electronic Supplementary Information

Reductive linear- and cyclo-trimerization of isocyanides using an Al–Al-bonded compound

Weixing Chen,^a Yanxia Zhao,^{*a} Wenhua Xu,^a Ji-Hu Su,^b Lingyi Shen,^a Li Liu,^a Biao Wu,^a and Xiao-Juan Yang^{*a}

^a *Key Laboratory of Synthetic and Natural Functional Molecule Chemistry of the Ministry of Education, College of Chemistry and Materials Science, Northwest University, Xi'an 710069, China*

**Correspondence: zhaoyx@nwu.edu.cn; yangxiaojuan@nwu.edu.cn*

^b *Hefei National Laboratory for Physical Sciences at the Microscale and Department of Modern Physics, CAS Key Laboratory of Microscale Magnetic Resonance, University of Science and Technology of China, Hefei 230026, China*

Table of Contents

S1. Experimental Details

S2. X-ray Crystallographic Analysis

S3. Theoretical Calculations

S4. References

S1. Experimental Details

General Procedures

All of the reactions and manipulations of air- and moisture-sensitive compounds were carried out under argon or nitrogen with standard Schlenk or drybox techniques. The solvents (toluene and THF) were dried using appropriate methods and were distilled under argon prior to use. Benzene-*d*₆ was dried over Na/K alloy. The α -diimine ligand L was prepared according to literature procedures.¹ Sodium metal, anhydrous aluminum chloride (AlCl₃) and *tert*-butyl isocyanide (*t*BuNC) were purchased from Alfa Aesar. NMR spectra were recorded on a Mercury Plus-400 spectrometer. Elemental analyses were performed with an Elementar VarioEL III instrument. EPR spectra were recorded on a Bruker E500-9.5/12 spectrometer at room temperature by using a standard resonance cavity. IR spectra were recorded using a Nicolet AVATAR 360 FT-IR spectrometer.

Synthesis

[LAl(*t*BuN=C–C=N*t*Bu)AlL] (2)

*t*BuNC (0.168 g, 2.0 mmol) was added to a solution of [L(THF)Al–Al(THF)L] (1)² (1.0 mmol) in 30 mL of toluene, and the mixture was stirred at r.t. for 12h, upon which the color changed from deep-red to brown. Then the reaction mixture was filtered and the filtrate was concentrated to about 5 mL. Light-green crystals were grown at –20 °C (0.690 g, 67%). ¹H NMR (400 MHz, C₆D₆): δ = 0.75 (d, *J* = 6.7 Hz, 6H; CH(CH₃)₂), 1.15 (s, 9H; C(CH₃)₃), 1.18 (d, *J* = 6.8 Hz, 6H; CH(CH₃)₂), 1.31 (d, *J* = 6.5 Hz, 6H; CH(CH₃)₂), 1.35 (d, *J* = 6.6 Hz, 6H; CH(CH₃)₂), 1.57 (s, 6H CCH₃), 3.31 (m, 2H; CH(CH₃)₂), 3.71 (m, 2H; CH(CH₃)₂), 7.01–7.13 (m, 6H; Ar). ¹³C NMR (100.6 MHz, C₆D₆): δ = 14.8 (N–CCH₃), 24.5 (CH(CH₃)₂), 25.2 (CH(CH₃)₂), 25.5 (CH(CH₃)₂), 27.6 (CH(CH₃)₂), 28.7 (C(CH₃)₃), 60.2 (C(CH₃)₃), 120.4 (N–CCH₃), 123.1, 123.6, 124.4, 125.3, 128.2, 129.0, 142.8, 145.4 (Ar), 146.8 ppm (*t*BuNC=CN*t*Bu). IR (Nujol, cm⁻¹): 3050 w, 2958 s, 2870 s, 1622 w, 1585 w, 1458 m, 1429 s, 1379 m, 1321 m, 1254 s, 1217 m, 1178 m, 1120 m, 1055 s, 945 m, 899 m, 787 m, 644 w, 563 m. Elemental analysis calcd. for C₆₆H₉₈Al₂N₆ (1029.46): C 77.00; H 9.59; N 8.16. Found: C 77.34, H 9.43 N 7.91%.

[Na]⁺[LAl{(tBuNC)₃}AlL]⁻ (**3**) and (**4**)

0.084 g (1.0 mmol) of *t*BuNC was added to a solution of 1.0 mmol of **2** and 1.0 mmol of Na metal in 30 mL toluene. The color of the solution changed from green to red-brown. The mixture was filtered and all volatiles were removed in vacuum, and the residue was dissolved in THF (10 mL). Purple block crystals of compound **3** were crystallized in several days. Yield: 0.540 g (34 %). EPR (THF, 295 K): $g = 2.004$. IR (Nujol, cm⁻¹): 3026 m, 2971 s, 2924 s, 2864 s, 1649 w, 1494 s, 1460 s, 1417 s, 1070 s, 910 m, 866 m, 731 s, 694 m, 565 m, 717 m, 792 m, 928 m, 1033 m, 1151 m, 1214 m, 1244 m, 1380 s, 1491 w, 1636 w. Elemental analysis calcd. for C₇₁H₁₀₇Al₂N₇Na(THF)₅·toluene (C₉₈H₁₅₅Al₂N₇NaO₅ 1588.23): C 74.11, H 9.84, N 6.17; found: C 73.80, H 9.69, N 6.03%. The mother liquor was concentrated and cooled to -20 °C to yield red crystals of **4** in 25% yield (0.388 g). **For complex 4:** EPR (THF, 295 K): $g = 2.005$, HFCs constants: $A(2 \times ^{27}\text{Al}) = A(3 \times ^{14}\text{N} = 6.75)$. IR (Nujol, cm⁻¹): 3059 m, 3028 s, 2968 m, 2922 m, 2870 m, 1603 w, 1495 s, 1462 m, 1385 m, 1245 w, 1206 w, 1174 w, 1078 w, 1034 w, 729 s, 694 s, 465 m. Elemental analysis calcd. for C₇₁H₁₀₇Al₂N₇Na(THF)_{4.5}·toluene (C₉₆H₁₅₁Al₂N₇NaO_{4.5} 1552.18): C 74.28, H 9.81, N 6.32; found: C 74.43, H 9.65, N 6.28%.

[Na]⁺[LAl{μ-η¹:η²-cyclo-(tBuNC)₃}Al(C≡N)L]⁻ (**5**)

Complex **5** was prepared by a similar procedure to that employed for **3** and **4**. *t*BuNC (0.168 g, 2.0 mmol) was added to a solution of **2** (1.0 mmol) and Na metal in toluene (25 mL) (Reaction of **1** with 4.0 equiv. *t*BuNC and Na metal can also produce the compound **5**). The resultant brown solution was stirred at ambient temperature for 3 days. The mixture was filtered, and the red filtrate was concentrated. Yellow crystals were grown from a toluene-THF solution at -20 °C for 1 week (0.813 g, 59%). ¹H NMR (400 MHz, C₆D₆): δ = 0.57 (s, 9H; C(CH₃)₃), 1.02 (d, $J = 4.3$ Hz, 6H; CH(CH₃)₂), 1.24 (d, $J = 6.7$ Hz, 6H; CH(CH₃)₂), 1.26 (d, $J = 12.4$ Hz, 6H; CH(CH₃)₂), 1.29 (d, $J = 6.8$ Hz, 6H; CH(CH₃)₂), 1.35 (d, $J = 3.3$ Hz, 6H; CH(CH₃)₂), 1.41 (d, $J = 6.8$ Hz, 6H; CH(CH₃)₂), 1.44 (d, $J = 6.6$ Hz, 6H; CH(CH₃)₂), 1.48 (d, $J = 6.7$ Hz, 6H; CH(CH₃)₂), 1.59 (s, 9H; C(CH₃)₃), 1.72 (s, 6H; CCH₃), 1.75 (s, 9H; C(CH₃)₃), 1.78 (s, 6H; CCH₃), 3.84 (m, 2H; CH(CH₃)₂), 3.90 (s, 2H; CH(CH₃)₂), 4.16 (m, 2H; CH(CH₃)₂), 4.28 (m, 2H; CH(CH₃)₂), 7.01–7.22

(m, 12H; Ph). ^{13}C NMR (C_6D_6): δ = 15.6 (N-CCH₃), 16.1 (N-CCH₃), 25.1 (CH(CH₃)₂), 25.2 (CH(CH₃)₂), 25.3 (CH(CH₃)₂), 25.4 (CH(CH₃)₂), 27.2 (CH(CH₃)₂), 27.5 (CH(CH₃)₂), 30.5 (C(CH₃)₃), 31.3 (C(CH₃)₃), 31.6 (C(CH₃)₃), 52.2 (C(CH₃)₃), 52.6 (C(CH₃)₃), 54.9 (C(CH₃)₃), 103.7 (C₃N₃), 121.7 (C₃N₃), 123.4 (C₃N₃), 123.8 (N-CCH₃), 124.8, 125.7, 128.6, 129.3, 136.9, 137.9, 138.4, 145.9 (ph), 160.2 (N≡C). IR (Nujol, cm^{-1}): 3049 w, 2957 s, 2853 s, 2180 w, 1620 w, 1495 m, 1462 s, 1377 s, 1286 m, 1254 m, 1211 m, 1173 m, 1042 w, 939 m, 914 w, 789 m, 727 m, 569 w. Elemental analysis calcd for $\text{C}_{80}\text{H}_{123}\text{Al}_2\text{N}_8\text{NaO}_2\cdot\text{THF}$ ($\text{C}_{84}\text{H}_{131}\text{Al}_2\text{N}_8\text{NaO}_3$ 1377.91): C 73.22; H 9.58; N 8.13; found: C 73.52, H 9.43 N 8.08%.

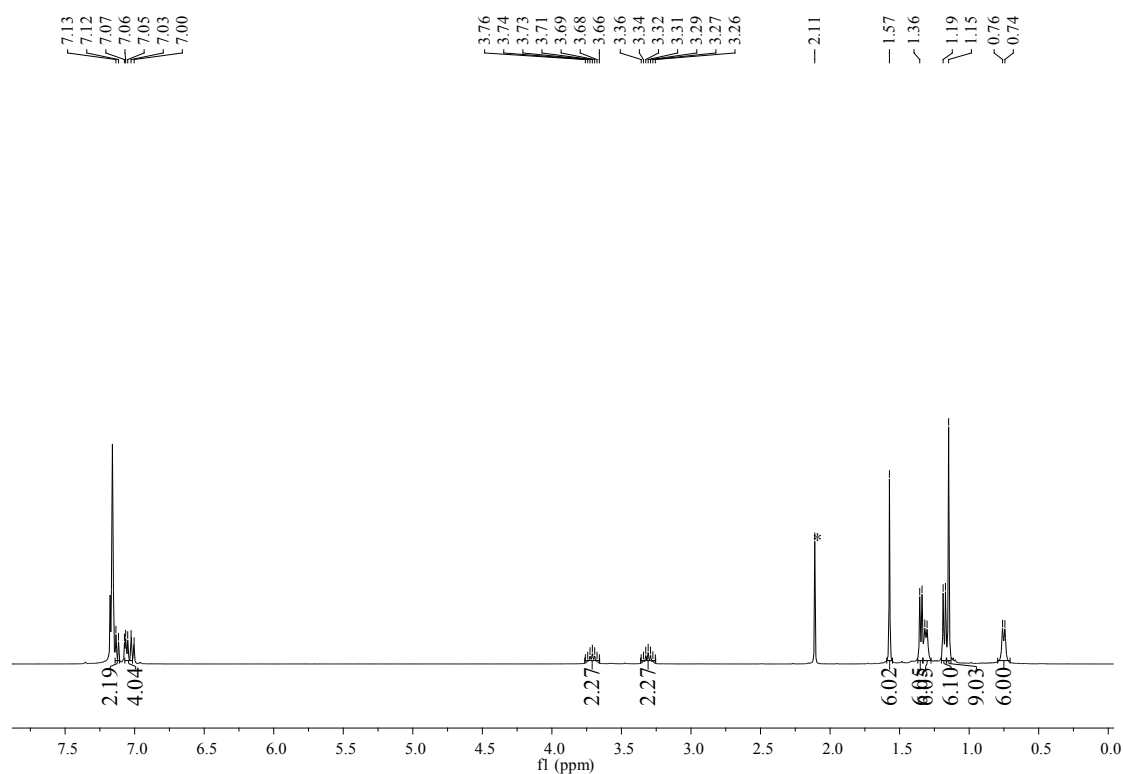


Fig. S1. ^1H NMR spectrum of **2** in C_6D_6 .

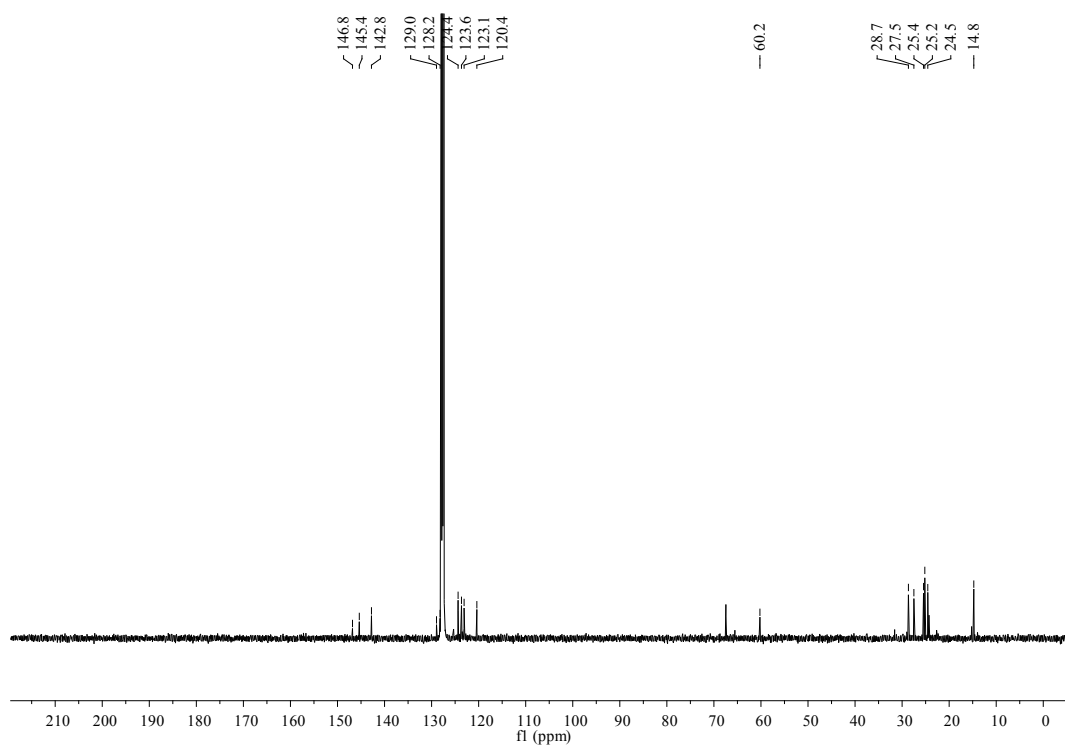


Fig. S2. ^{13}C NMR spectrum of **2** in C_6D_6 .

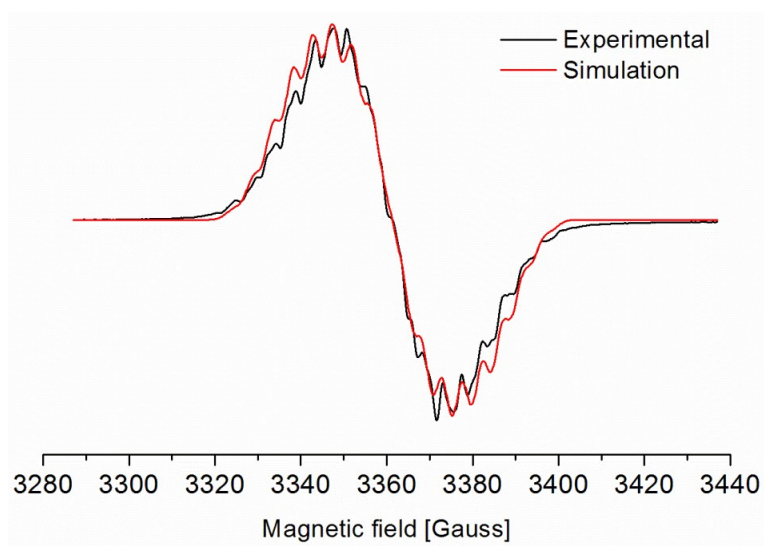


Fig. S3. X-band EPR spectrum of **3** in THF at room temperature. Experimental conditions: frequency 9.422 GHz; the red line is simulated ($A(2 \times ^{14}\text{N}) = A(2 \times ^{13}\text{Al}) = 4.60$ G and $A(1 \times ^{14}\text{N}) = 3.10$ G; $g = 2.004$).

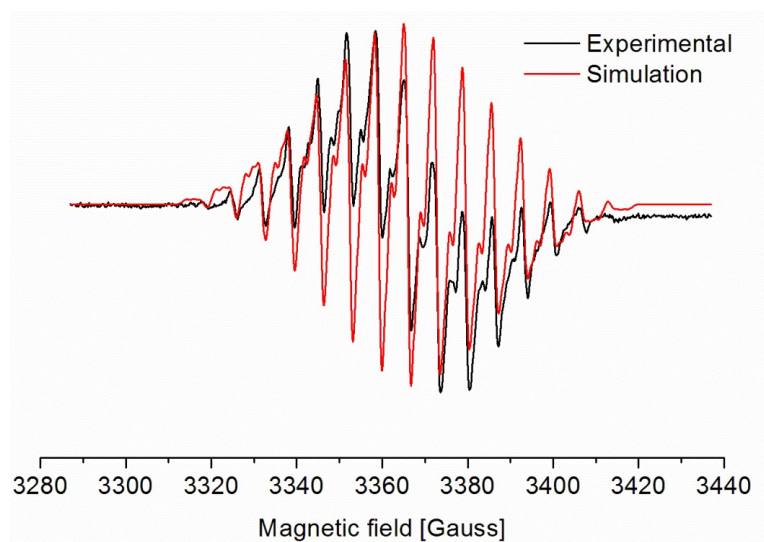


Fig. S4. X-band EPR spectrum of **4** in THF at room temperature. Experimental conditions: frequency 9.432 GHz; the red line is simulated ($A(1 \times {}^{14}\text{N}) = A(2 \times {}^{13}\text{Al}) = 6.80$ G, and $A(2 \times {}^{14}\text{N}) = 1.70$ G; $g = 2.005$).

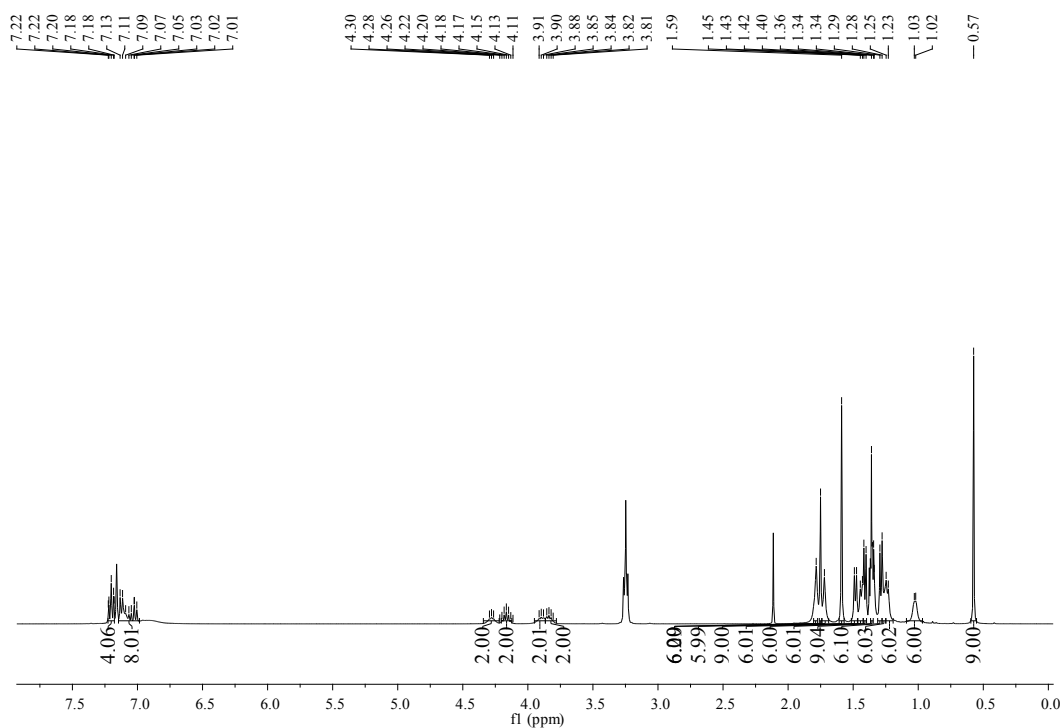


Fig. S5. ${}^1\text{H}$ NMR spectrum of compound **5** in C_6D_6 .

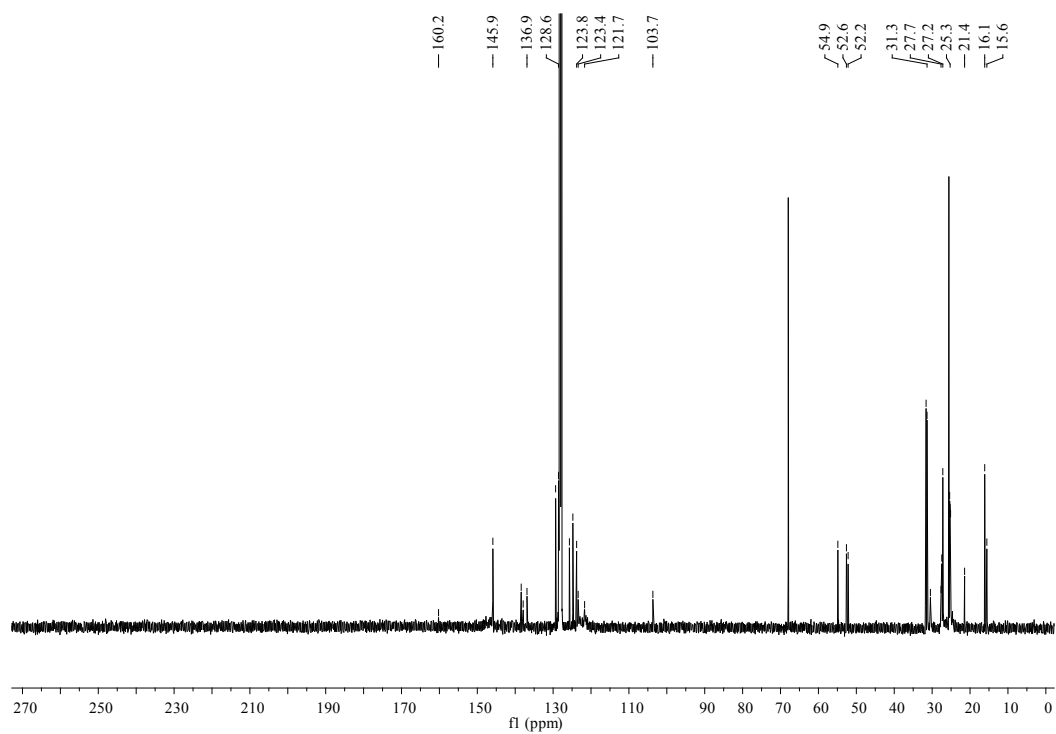


Fig. S6 ^{13}C NMR spectrum of compound **5** in C_6D_6 .

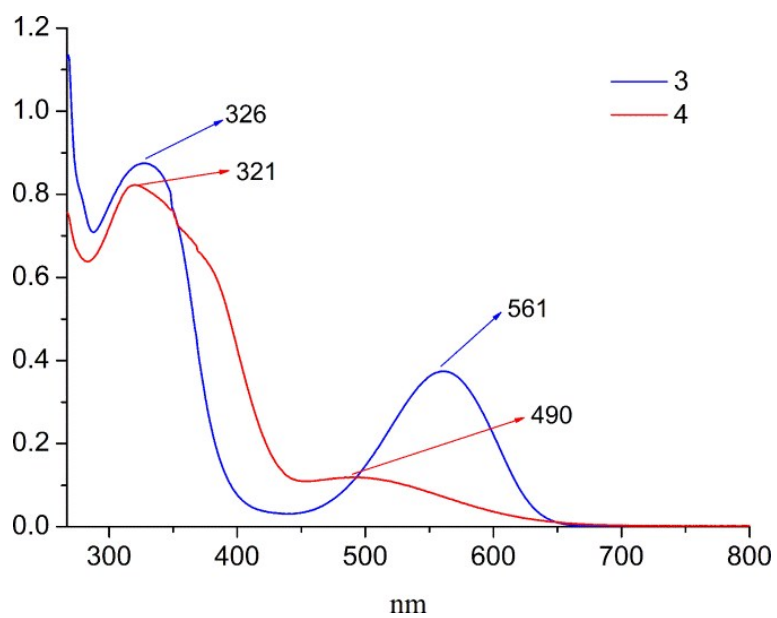


Fig. S7. UV-Vis spectra of **3** and **4** in THF.

S2. X-ray Crystallographic Analysis

Diffraction data for complexes **2–5** were collected on a Bruker SMART APEX II diffractometer at 153 K with graphite-monochromated Mo K α radiation ($\lambda = 0.71073$ Å). An empirical absorption correction using SADABS was applied for all data.³ The structures were solved and refined to convergence on F^2 for all independent reflections by the full-matrix least squares method using the SHELXL–2014 programs⁴ and OLEX2 1.2.⁵ **In compound 2**, there is a VOID which made a B-alert, but the largest residual electron density is 0.62 e/Å³, and the free solvent molecule was not identified. **In compound 3**, severely disordered atoms in solvent molecules (THF and toluene) made five B-alerts. **In compound 4**, some atoms, such as N5, C57 and C55 are disordered into two positions to N5 (occupancies of 80%, N5A (20%), C57 (60%), C57A (40%) and C55 (50%), C55A (50%). Moreover, some atoms in the solvents are disordered and display unusual thermal parameters, which caused the level B alerts. **In compound 5**, about 4.5 molecules of THF (about 1 THF molecules per formula, $Z = 4$) are co-crystallized, with the corresponding electron density (180 electrons) being removed using the SQUEEZE routine implemented within the software program PLATON,⁶ and the resulting .fab file was processed with OLEX2 1.2 using the ABIN instruction. Crystallographic data and refinement details for compounds **2–5** are given in Table S1. CCDC numbers 1897325 (for **2**), 1897328 (for **3**), 1897329 (for **4**), and 1897330 (for **5**). These data can be obtained free of charge from the Cambridge Crystallographic Data Centre www.ccdc.cam.ac.uk/data_request/cif.

Table S1. Crystallographic data and refinement details for compounds **2–5**.

Compound	2	3	4	5
Empirical formula	C ₆₆ H ₉₈ Al ₂ N ₆	C ₇₁ H ₁₀₇ Al ₂ N ₇ ·Na(THF) ₅ ·toluene	[C ₇₁ H ₁₀₇ Al ₂ N ₇ ·Na(THF) _{4.5} ·toluene]*2	C ₈₀ H ₁₂₃ Al ₂ N ₈ NaO ₂ ·THF
Fw	1029.46	1588.23	3104.36	1377.91
Crystal system	Monoclinic	Triclinic	Monoclinic	Monoclinic
Space group	<i>P2₁/n</i>	<i>P</i> -1	<i>C2/c</i>	<i>P2₁/n</i>
<i>a</i> /Å	10.966(3)	15.6041(9)	26.810(5)	17.844(9)
<i>b</i> /Å	16.053(4)	18.0836(11)	26.916(5)	26.227(14)
<i>c</i> /Å	18.226(4)	18.4143(12)	28.097(6)	20.493(13)
α /°	90	76.535(2)	90	90
β /°	97.379(3)	71.288(2)	111.31(3)	108.599(16)
γ /°	90	85.598(2)	90	90
<i>V</i> /Å ³	3181.7(13)	4786.2(5)	18889(7)	9089(9)
<i>Z</i>	2	2	4	4
<i>D</i> _{calc} /g cm ⁻³	1.075	1.102	1.092	1.007
<i>F</i> (000)	1124	1738	6792	3008
μ /mm ⁻¹	0.088	0.088	0.087	0.083
θ range	1.697–25.000	1.739–25.358	2.225–24.748	2.236–25.042
Reflns collected	5526	63407	103837	112677

Independent reflns	5526	17473	16063	15994
Reflns [$I > 2\sigma(I)$]	3831	10463	9261	8520
R_{int}	0.0890	0.0779	0.1012	0.0822
$R_1; wR_2$ [$I > 2\sigma(I)$]	0.0830; 0.2053	0.1000; 0.2081	0.0808; 0.1749	0.0619; 0.1358
$R_1; wR_2$ (all data)	0.1299; 0.2209	0.1552; 0.2376	0.1474; 0.2150	0.1307; 0.1626
GOF (F^2)	1.038	1.022	1.004	1.013

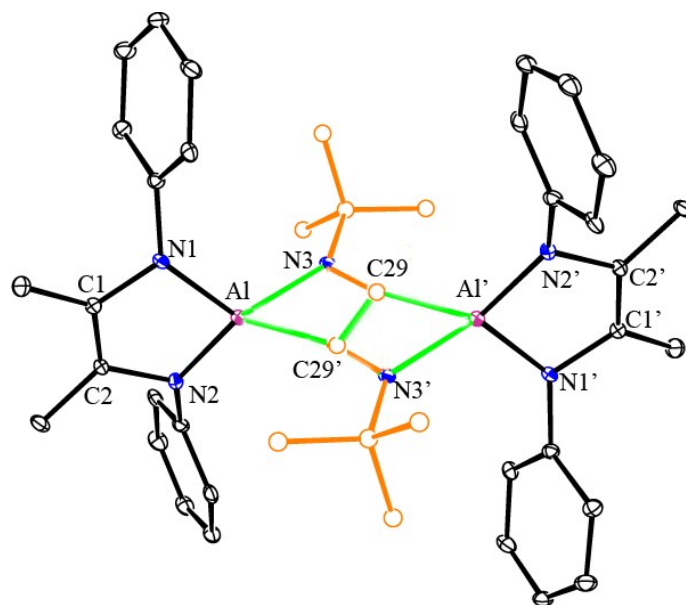


Fig. S8. Molecular structure of **2** (thermal ellipsoids are set at the 20% probability level; H atoms and *i*Pr groups of L are omitted for clarity, and the C atom in tBuNC molecules are drawn as smaller spheres, the new bonds were marked in green). Selected bond lengths (Å) and angles (°): Al–N1 1.814(5), Al–N2 1.805(5), Al–N3 2.003(5), Al–C29' 2.037(6), N3–C29 1.313(7), C29–C29' 1.472(1), N1–C1 1.454(7), N2–C2 1.430(7), C1–C2 1.334(8), N1–Al–N2 92.9(2), N2–Al–N3 117.9(2), N1–Al–C29' 126.6(2), N3–Al–C29' 67.8(2), N3–C29–C29' 107.9(6), Al–C29'–C29 89.1(4), Al–N3–C29 95.2(3). Symmetry code: $x-1, y-1, z-1$.

Crystal Structure and Spectroscopic Characterization of **2**

In the dimerization product **2** (Figure S8), the geometry of the central C–C coupled unit is indicative of an essentially localized 1,4-diazabutadiene-2,3-diyl fragment $[\text{RN}=\text{C}=\text{C}=\text{NR}]^{2-}$, which adopts a *trans* conformation and is C,N-chelating to two [AIL] moieties, with the N3–C29 distance of 1.313(7) Å and C29–C29' of 1.472(1) Å. The $\text{Al}_2\text{C}_2\text{N}_2$ core is almost planar, and the aluminum atoms deviate from the C_2N_2 plane by 0.07 Å. The dative $\text{N}\rightarrow\text{Al}$ (2.003(5) Å)

interaction in **2** is significantly longer than the covalent Al–N (1.814(5) and 1.805(5) Å) bonds within the [AlL²⁻] cycles, which is much similar to that in the congeneric dialuminum species Dis₂Al(*t*BuN=C–C=N*t*Bu)AlDis₂ (2.040(2) Å). The Al–C distances (2.037(6) Å) are also comparable to those in the latter (2.075(2) Å).⁷ The IR spectrum of **2** exhibits the double-bond C=N stretching mode at 1622 cm⁻¹, which is much smaller than that of the triple bond in *t*BuNC (2134 cm⁻¹).⁸ The UV-Vis spectrum of **2** (Figure S10) only show one absorption at 330 nm (Figures S16), corresponding to α -diimine L. Natural population analysis (NPA) indicates that the natural charge on Al (1.81) is more positive than in **1** (1.13), while the central [*t*BuNCCN*t*Bu] core shows negative charges of –0.91 e (in **2'**) (Table S2). These calculation results suggest the existence of Al(III), L²⁻, and the (*t*BuN=C–C=N*t*Bu)²⁻ anions compound **2**.

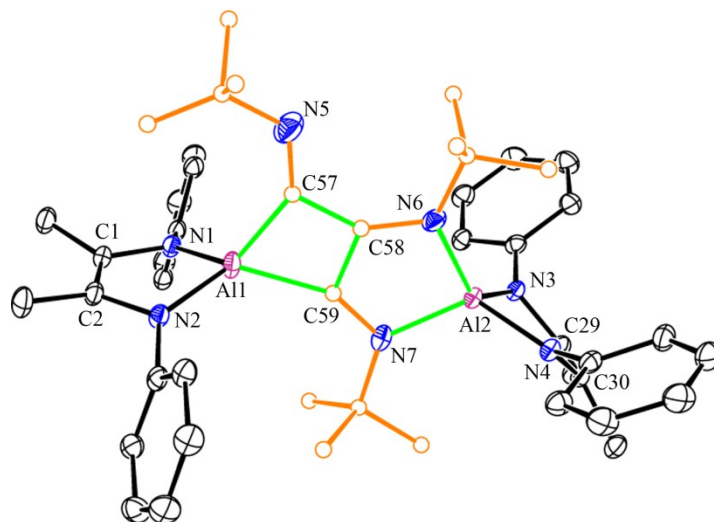


Fig. S9. Molecular structure of the [LAl{(*t*BuNC)₃}Al]⁻ anion in **4** (thermal ellipsoids are set at the 20% probability level; H atoms, *t*Pr groups of L, and Na(THF)₅⁺ cation are omitted for clarity). Selected bond lengths (Å) and angles (°): Al1–N1 1.862(3), Al1–N2 1.864(3), Al1–C57 1.881(7), Al1–C59 2.016(4), Al2–N3 1.862(3), Al2–N4 1.873(3), Al2–N6 1.852(3), Al2–N7 1.933(3), N6–C58 1.391(5), N7–C59 1.331(5), C57–C58 1.475(7), C58–C59 1.427(6), N1–C1 1.432(4), N2–C2 1.433(5), C1–C2 1.349(5), N3–C29 1.434(4), N4–C30 1.439(5), C29–C30 1.339(5); N1–Al1–N2 89.47(1), C57–Al1–C59 67.9(2), N5–C57–Al1 138.9(5), C57–C58–C59 97.4(4), N3–Al2–N4 89.68(14), N6–Al2–N7 87.04(15), C58–N6–Al2 109.8(3), C59–N7–Al2 111.5(3), N6–C58–C59 117.5(4), N7–C59–C58 113.9(4).

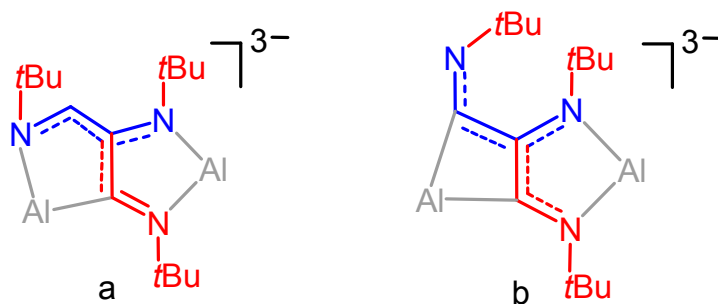


Chart S1. Conformation of the linear trimerized isocyanide fragment $[(t\text{BuNC})_3]^{3-}$ in complexes **3** (a) and **4** (b).

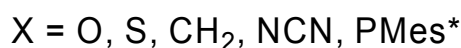
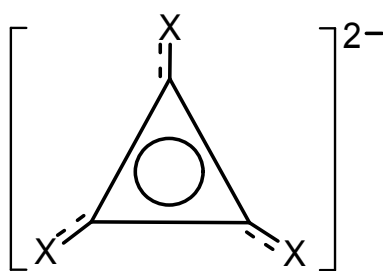


Chart S2. The dianionic [3]radialene derivatives.

S3. Theoretical Calculations

Structure optimization for the model compounds $[\text{L}'^{2-}\text{Al}^{\text{III}}(\text{tBuN}=\text{C}=\text{C}=\text{NtBu})_2\text{Al}^{\text{III}}\text{L}'^{2-}]$ (**2'**, $\text{L}' = (\text{PhNCMe})_2$), $[\text{L}'^{2-}\text{Al}^{\text{III}}\{(\text{tBuNC})_3\}^{3-}\text{Al}^{\text{III}}\text{L}'^{2-}]$ (**3'** and **4'**), and $([\text{Na}\cdot 2\text{H}_2\text{O}]^+[\text{L}'^{2-}\text{Al}^{\text{III}}\{\mu\text{-}\eta^1:\eta^2\text{-}(\text{tBuNC})_3\}^{2-}\text{Al}^{\text{III}}(\text{C}\equiv\text{N})\text{L}'^{2-}])$ (**5'**), in which the 2,6-*i*Pr₂C₆H₃ groups in L were replaced by Ph groups, was carried out at the DFT (B3LYP) level with a 6-31G*^{9,10} basis set using the Gaussian 09 program.¹¹ Figures S12 and S13 show the optimized geometries, which reproduce the experimental data of **2–5** reasonably well. The atomic populations, bonding orbitals and Wiberg bond orders were obtained with NBO method.^{12–14} Time-dependent DFT calculations were carried out at the B3LYP/6-31g*. The NICS values¹⁵ were estimated using the gauge-independent atomic orbital (GIAO) method^{16–19} at the B3LYP/6-31G* level.

As mentioned in the main text, reaction of **2** with 1 equiv of *t*BuNC and Na produced complexes $[\text{Na}]^+[\text{LAl}\{(\text{tBuNC})_3\}\text{AlL}]^-$ (**3** and **4**), while in the absence of Na, the possible product of neutral $[\text{LAl}\{(\text{tBuNC})_3\}\text{AlL}]$ was not isolated. Here the DFT results demonstrate that compound **3-Na** in the (doublet) monoanionic $[\text{L}^{2-}\text{Al}^{\text{III}}\{(\text{tBuNC})_3\}^{3-}\text{Al}^{\text{III}}\text{L}^{2-}]^-$ form is much more

stable than the possible neutral form (singlet $[L^2-Al^{III}\{(tBuNC)_3\}^2-Al^{III}L^2-]$ and triplet $[L^--Al^{III}\{(tBuNC)_3\}^3-Al^{III}L^2-]$), by 57.14 and 52.29 kcal/mol, respectively (Tables S3 and S4), which is consistent with the experimental observations. Moreover, for isomers **3** and **4**, which are isolated from the same reaction mixture, DFT results show that **4** exhibits a slightly lower energy than **3** ($\Delta E = 5.27$ kcal/mol). However, interconversion between the two products has not been observed even at elevated temperatures.

Table S2. Natural charges (e) of the model compounds **3'**–**5'**.

Compound	2'	3'	4'	5'
Al	1.8092	1.8327, 1.9882	2.0477, 1.7702	2.0226, 1.8623
L	-1.3556	-1.4810, -1.4955	-1.5261, -1.4826	-1.4842, -1.4407
(<i>t</i> BuNC) ₃	-0.9071	-1.8443	-1.8093	-1.2439, -0.6325(NC)

Table S3. Natural charges of the model compounds: monoanionic doublet $[L^2-Al^{III}\{(tBuNC)_3\}^3-Al^{III}L^2-]$ (**3-Na**), neutral singlet $[L^2-Al^{III}\{(tBuNC)_3\}^2-Al^{III}L^2-]$ and triplet $[L^--Al^{III}\{(tBuNC)_3\}^3-Al^{III}L^2-]$

Compound	$[L^2-Al^{III}\{(tBuNC)_3\}^3-Al^{III}L^2-]$	$[L^2-Al^{III}\{(tBuNC)_3\}^2-Al^{III}L^2-]$	$[L^--Al^{III}\{(tBuNC)_3\}^3-Al^{III}L^2-]$
Al	1.9004, 2.0505	1.9050, 2.0470	1.892, 2.0570
L	-1.5094, -1.5263	-1.2610, -1.3007	-0.7336, -1.485
(<i>t</i> BuNC) ₃	-1.9152	-1.3902	-1.7304

Table S4. Relative energies of compounds in monoanionic doublet $[L^2-Al^{III}\{(tBuNC)_3\}^3-Al^{III}L^2-]$ (**3-Na**), neutral singlet $[L^2-Al^{III}\{(tBuNC)_3\}^2-Al^{III}L^2-]$ and triplet $[L^--Al^{III}\{(tBuNC)_3\}^3-Al^{III}L^2-]$

Compound	Spin multiplicity	Energy (E, a.u.)	ΔE (kcal/mol)	Gibbs free energy (G, a.u.)	ΔG (kcal/mol)
$[L^2-Al^{III}\{(tBuNC)_3\}^3-Al^{III}L^2-]$	2	-2694.91140174	0	-2694.038068	0
$[L^2-Al^{III}\{(tBuNC)_3\}^2-Al^{III}L^2-]$	1	-2694.82033679	57.14	-2693.944736	58.56
$[L^--Al^{III}\{(tBuNC)_3\}^3-Al^{III}L^2-]$	3	-2694.82806846	52.29	-2693.953723	53.24

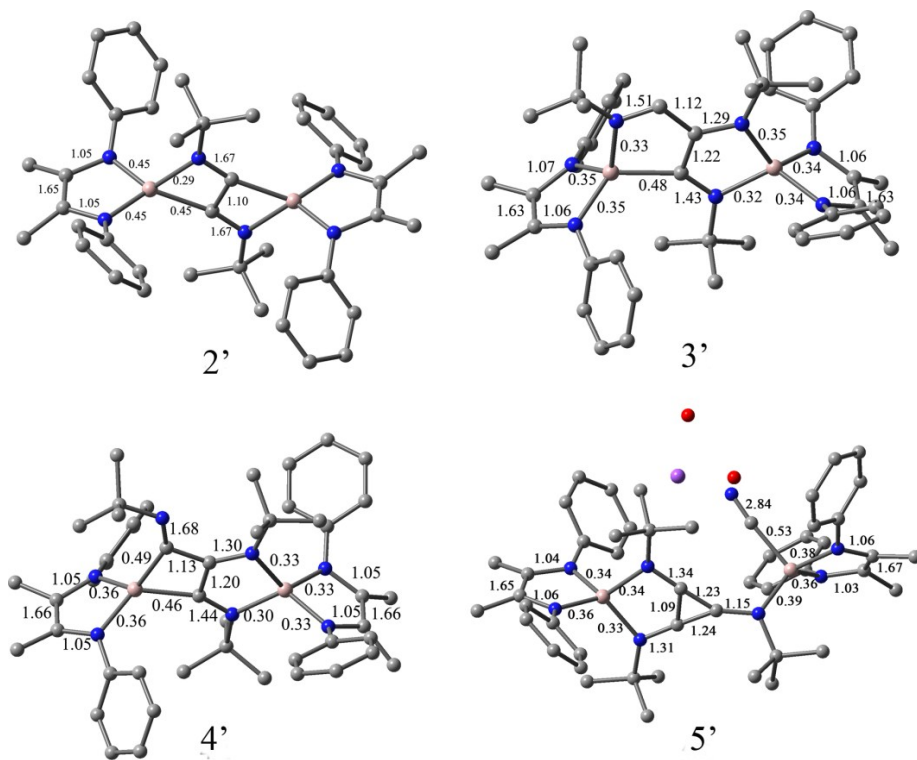


Fig. S10. Optimized structures of 2'–5' labelled with selected bond orders.

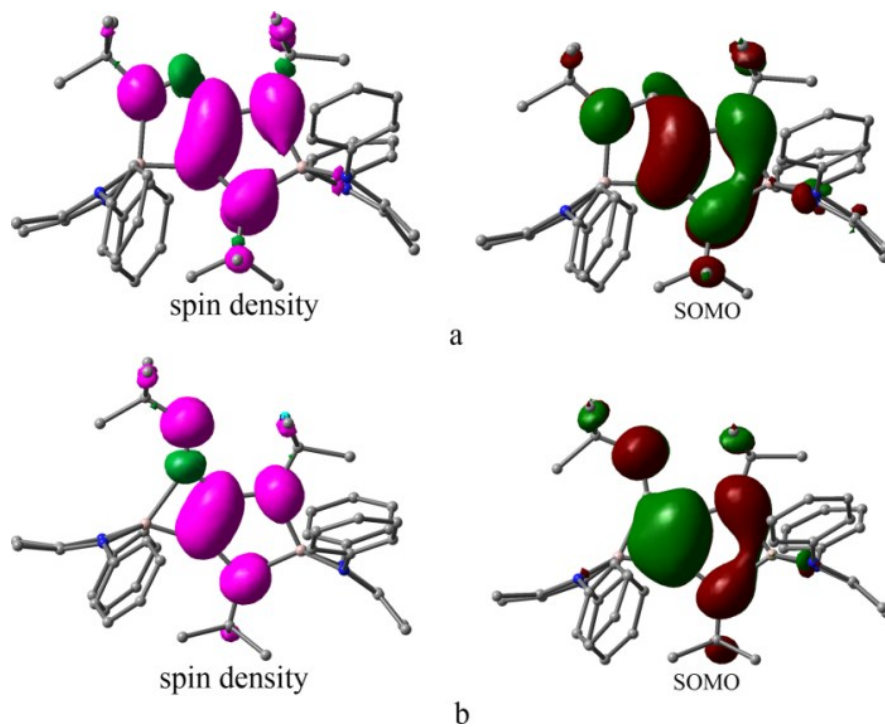
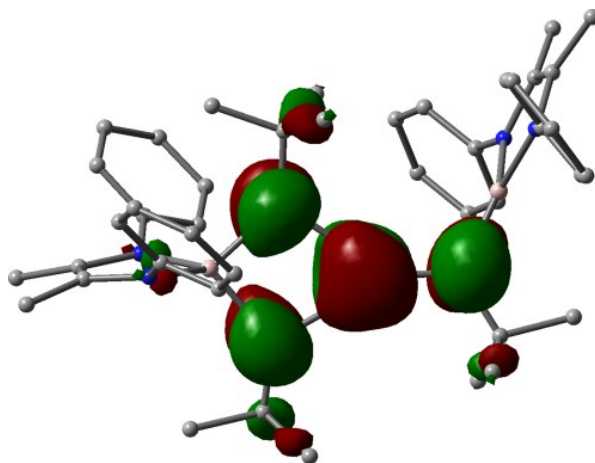


Fig. S11. The Mulliken spin density distribution and SOMO of 3 (a) and 4 (b).



HOMO-3

Fig. S12. The HOMO-3 of **5** showing a π -type orbital over the C₃ ring.

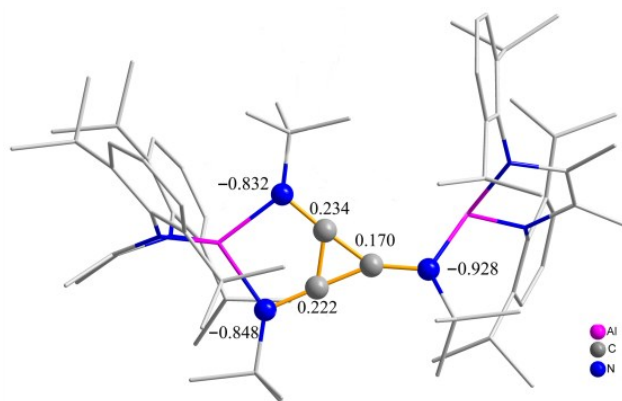


Fig. 13. NPA charges in **5** (H atoms and Na(THF)₂⁺ cation are omitted for clarity).

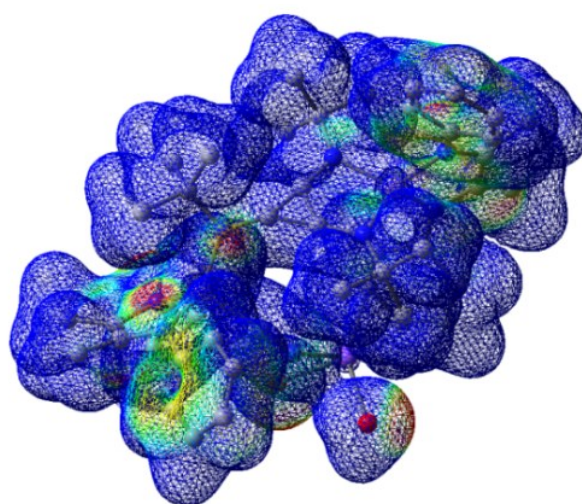


Fig. S14. Electronic Static Potential (ESP) of compound **5**.

UV-Vis spectra

In order to gain insight into the origin of the bands of the UV-Vis spectra of **2–5**, TD-DFT calculations were conducted (Figures S12–S15 and Tables S5–S12). A number of low-energy transitions of significant intensity were predicted, and natural transition orbitals (NTOs) contributing to the transitions are shown in Tables S6, S8, S10 and S12. Electronic excitations are predicted at 506 nm (oscillator strength, $f_{\text{osc}} = 0.0260$) and 425 nm ($f_{\text{osc}} = 0.0267$), for compounds **3** and **4**, respectively, corresponding to the bands experimentally observed at, 561 and 490 nm, which are assigned to the delocalized radical anionic $[(t\text{BuNC})_3]^{3-}$ (**3** and **4**) framework. The other additional electronic transition was calculated at 326 nm ($f_{\text{osc}} = 0.2098$) and 326 nm ($f_{\text{osc}} = 0.5459$) which accounts for the band experimentally detected at 326 and 321 nm for compounds **3** and **4** respectively. The donor and acceptor orbitals for these transitions are delocalized over the α -diimine ligand framework (Figures S13, S14 and Tables S7–S10). While for compounds **2** and **5** without the organic radical, the UV-vis absorption spectra in THF reveal absorption bands at 330 and 320 nm. This is responsible for the light-green color of **2** and yellow of **5**, which are much lighter than the dark-purple color of **3** and deep-red **4**. TD-DFT analyses predict an intense band at 317 and 326 nm ($f_{\text{osc}} = 0.2150$) for **2** and **5** respectively, which are in agreement with the experimentally obtained values. The donor and acceptor orbitals for these transitions are delocalized over the α -diimine ligand (Figures S12, S15 and Tables S5, S6, S11 and S12).

IR spectrum of **5**

In the IR spectrum of complex **5**, the $\text{C}\equiv\text{N}$ stretch $\nu_{\text{C}\equiv\text{N}}$ is observed as a weak absorption at 2204 cm^{-1} (calculated 2279 cm^{-1}), which is shifted to a higher frequency compared to the free isocyanide (2134 cm^{-1}),⁸ as expected for $\text{C}\equiv\text{N}$ group coordinated as a σ donor in the absence of π -backbonding. This value is similar to that observed previously for aluminum isocyanide complexes $\text{R}_3\text{AlC}\equiv\text{N}t\text{Bu}$ (2218–2240 cm^{-1} , R = Me, Et, *t*Bu and Cp)⁸ and other cyanide complexes, such as $[\{(\text{DipNacnac})\text{Mg}(\mu\text{-CN})\}_3]$ (2281 and 2157 cm^{-1}),²⁰ $[(\text{Ar})_2\text{GeHC}\equiv\text{N}]$ (2177, calculated value 2326 cm^{-1}),²¹ and $[\{(\text{Me}_3\text{Si})_2\text{CH}\}_2\text{Al-CN}]_3$ (2185 cm^{-1}).²² Another very weak absorption at 1948 cm^{-1} in the IR spectrum may be assigned to the C_3 stretching based on DFT computations (calculated value 1898 cm^{-1}).

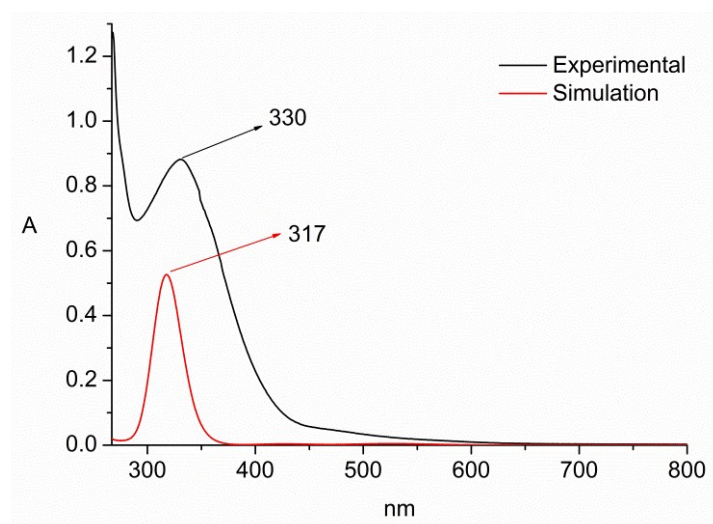


Fig. S15. Comparison of the experimental (in THF) and computational (B3LYP/6-31G*) UV-Vis spectra of **2**.

Table S5. The absorption wavelengths, oscillator strengths, main transition pairs and its amplitudes for selected excited states of compound **2'** at the B3LYP/6-31G* level of theory.

wavelength [nm]	f	transition	excitation amplitudes ^[a]
316.70	0.6915	184 HOMO-1 => 192 LUMO+6	0.51587
		185 HOMO => 195 LUMO+9	0.44005

[a] Only those excitation amplitudes greater than 0.3 are shown

Table S6. Natural Transition Orbitals (NTO) representing transitions contributing to the UV-Vis spectrum of **2'**.

Excited State	Properties	Electrons	Holes
Excited State 21			
	$f = 0.6915$		
	$\lambda_{\text{calc}} = 317$		
	$\lambda_{\text{exp}} = 330$		

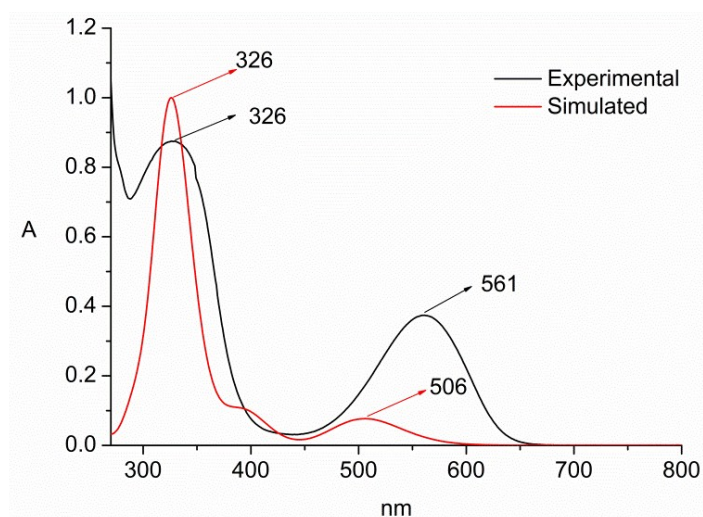


Fig. S16. The experimental (in THF) and computational (B3LYP/6-31G*) UV-Vis spectra of **3**.

Table S7. TD-DFT selected excitation energies and oscillator strengths for compound **3'** at the B3LYP/6-31G* level of theory.

wavelength [nm]	f	transition	excitation amplitudes ^[a]
325.80	0.2098	207 HOMO _{α} -2 => 212 LUMO _{α} +2	0.54174
		208 HOMO _{α} -1 => 215 LUMO _{α} +5	0.42225
		207 HOMO _{β} -1 => 215 LUMO _{β} +6	0.41563
506.41	0.0260	207 HOMO _{α} -2 => 210 LUMO _{α}	-0.63041
		204 HOMO _{β} -4 => 209 LUMO _{β}	0.32142
		205 HOMO _{β} -3 => 209 LUMO _{β}	0.67384

[a] Only those excitation amplitudes greater than 0.3 are shown.

Table S8. Natural Transition Orbitals (NTO) representing transitions contributing to the UV-Vis spectrum of **3'**.

Excited State Properties	Electrons	Holes
Excited State 6 (α)		
$f = 0.0260$		
$\lambda_{\text{calc}} = 561$		
$\lambda_{\text{exp}} = 506$		

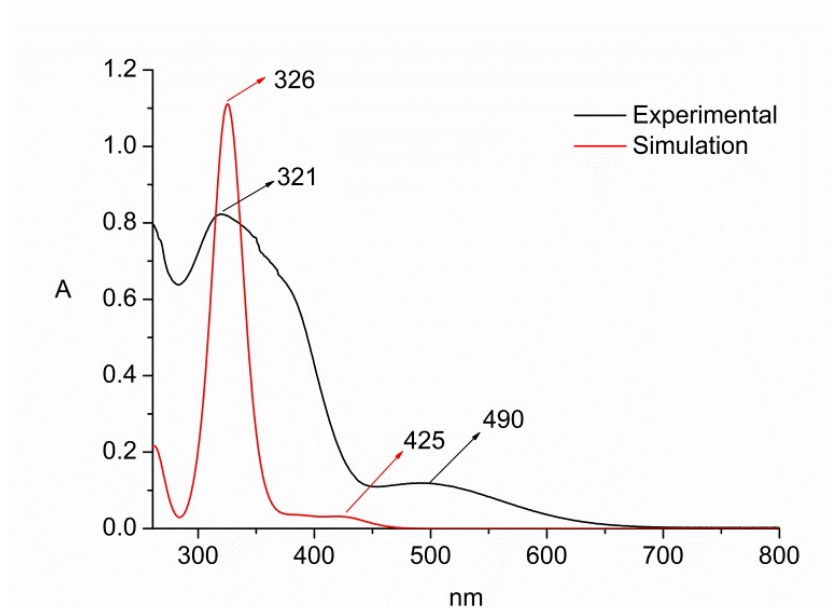
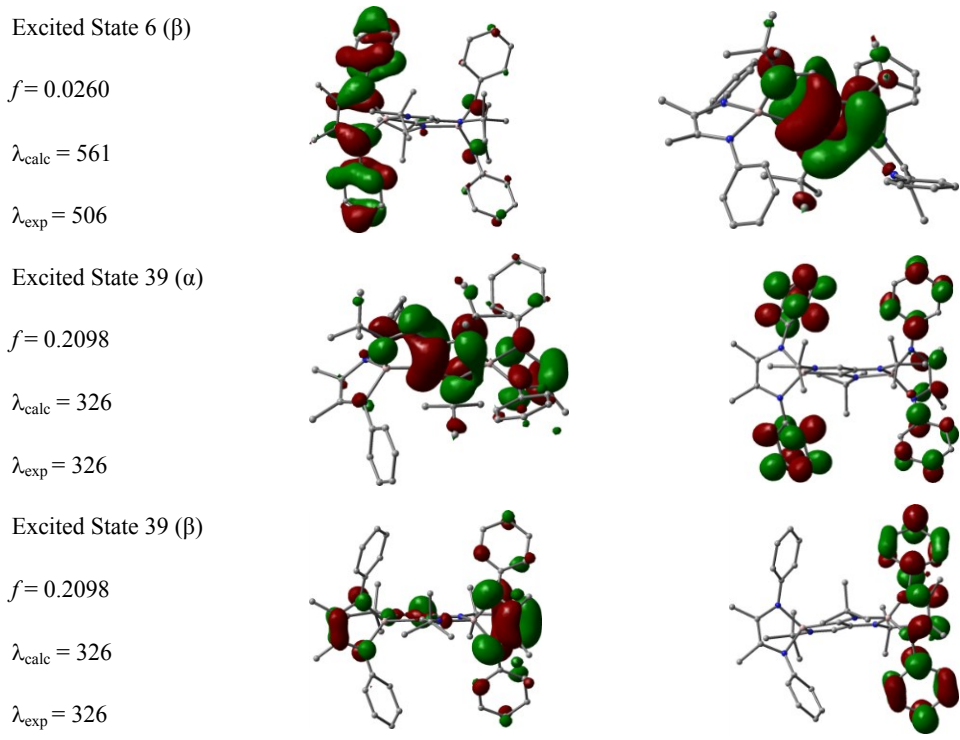


Fig. S17. The experimental (in THF) and computational (B3LYP/6-31G*) UV-Vis spectra of **4**.

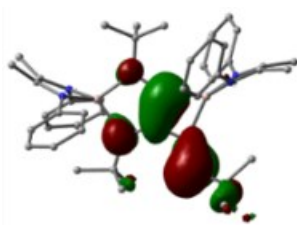
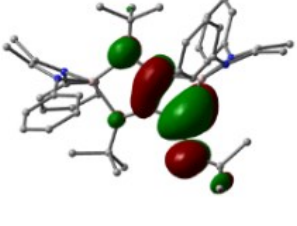
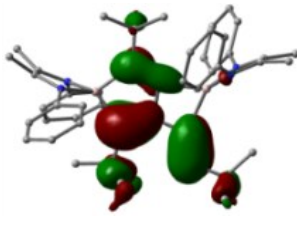
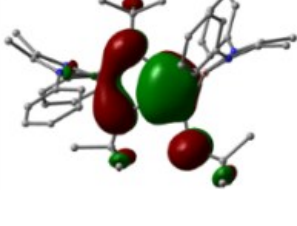
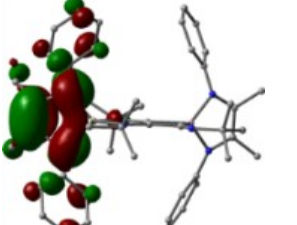
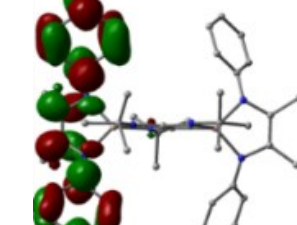
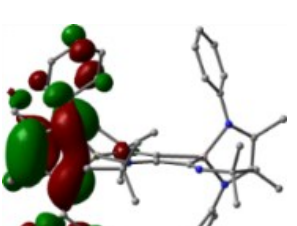
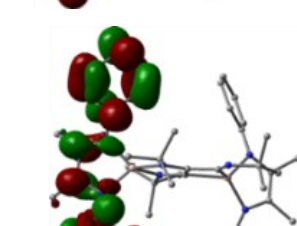
Table S9. TD-DFT selected excitation energies and oscillator strengths for compound **4'** at the B3LYP/6-31G* level of theory.

Wavelength [nm]	f	transition	excitation amplitudes ^[a]
325.62	0.5459	208 HOMO _{α-1} => 214 LUMO _{α+4}	0.42962

		208 HOMO _α -1 =>215 LUMO _α +5	0.49663
		207 HOMO _β -1 => 214 LUMO _β +5	0.63654
424.81	0.0267	197 HOMO _β -11 => 209LUMO _β	0.29413
		201 HOMO _β -7 => 209 LUMO _β	0.87133

[a] Only those excitation amplitudes greater than 0.3 are shown

Table S10. Natural Transition Orbitals (NTO) representing transitions contributing to the UV-Vis spectrum of **4'**.

Excited State	Properties	Electrons	Holes
Excited State 9 (α)	$f = 0.0267$ $\lambda_{\text{calc}} = 425$ $\lambda_{\text{exp}} = 490$		
Excited State 9 (β)	$f = 0.0267$ $\lambda_{\text{calc}} = 425$ $\lambda_{\text{exp}} = 490$		
Excited State 37 (α)	$f = 0.5459$ $\lambda_{\text{calc}} = 326$ $\lambda_{\text{exp}} = 321$		
Excited State 37 (β)	$f = 0.5459$ $\lambda_{\text{calc}} = 326$ $\lambda_{\text{exp}} = 321$		

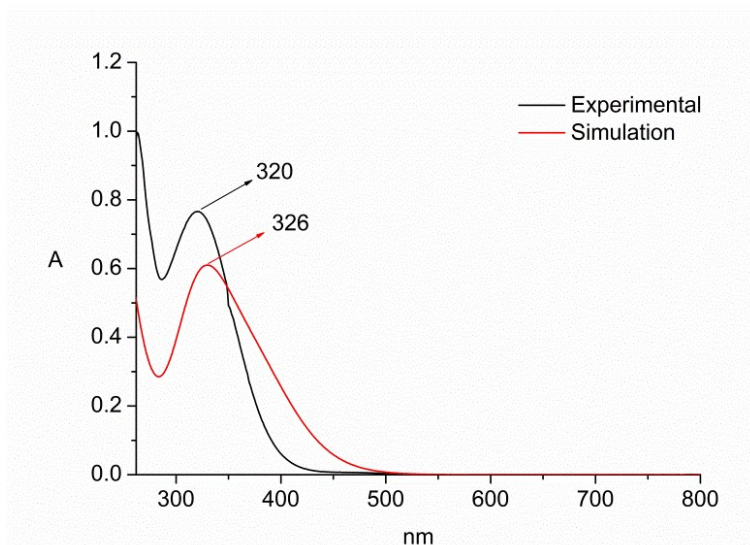


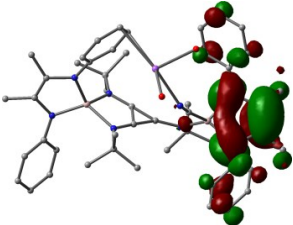
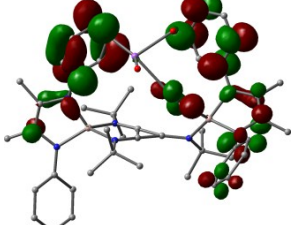
Fig. S18. The experimental (in THF) and computational (B3LYP/6-31G*) UV-Vis spectra of **5**.

Table S11. TD-DFT selected excitation energies and oscillator strengths for compound **5'** at the B3LYP/6-31G* level of theory.

Wavelength [nm]	f	transition	excitation amplitudes ^[a]
326.41	0.2150	229 HOMO-1 => 234 LUMO+3	0.37214
		229 HOMO-1 => 236 LUMO+5	0.35325
		229 HOMO-1 => 238 LUMO+7	-0.33277

[a] Only those excitation amplitudes greater than 0.3 are shown

Table S12. Natural Transition Orbitals (NTO) representing transitions contributing to the UV-Vis spectrum of **5'**.

Excited State	Properties	Electrons	Holes
Excited State 15	$f = 0.0267$ $\lambda_{\text{calc}} = 326$ $\lambda_{\text{exp}} = 320$		

S4 Reference

- 1 H. A. Zhong, J. A. Labinger and J. E. Bercaw, *J. Am. Chem. Soc.*, 2002, **124**, 1378–1399.
- 2 Y. Zhao, Y. Liu, L. Yang, J. G. Yu, S. Li, B. Wu and X. J. Yang, *Chem. – Eur. J.*, 2012, **18**, 6022–6030.
- 3 G. M. Sheldrick, Program SADABS: Area-Detector Absorption Correction, 1996, University of Göttingen, Germany.
- 4 G. M. Sheldrick, *Acta Crystallogr., Sect. C: Cryst. Struct. Commun.*, 2015, **71**, 3–8.
- 5 O. V. Dolomanov, L. J. Bourhis, R. J. Gildea, J. A. K. Howard and H. Puschmann, *J. Appl. Cryst.*, 2009, **42**, 339–341.
- 6 A. L. Spek, *Acta Cryst.*, 2015, **C71**, 9–18.
- 7 W. Uhl, U. Schütz, W. Hiller and M. Heckel, *Chem. Ber.*, 1994, **127**, 1587–1592.
- 8 N. B. Kingsley, K. Kirschbaum, J. A. Teprovich, R. A. Flowers and M. R. Mason, *Inorg. Chem.*, 2012, **51**, 2494–2502.
- 9 A. D. Becke, *J. Chem. Phys.*, 1993, **98**, 5648–5652.
- 10 C. Lee, W. Yang and R. G. Parr, *Phys. Rev. B.*, 1988, **37**, 785–789.
- 11 Gaussian 09, Revision C.1, M. J. Frisch, G. W. Trucks, H. B. Schlegel, G. E. Scuseria, M. A. Robb, J. R. Cheeseman, G. Scalmani, V. Barone, B. Mennucci, G. A. Petersson, H. Nakatsuji, M. Caricato, X. Li, H. P. Hratchian, A. F. Izmaylov, J. Bloino, G. Zheng, J. L. Sonnenberg, M. Hada, M. Ehara, K. Toyota, R. Fukuda, J. Hasegawa, M. Ishida, T. Nakajima, Y. Honda, O. Kitao, H. Nakai, T. Vreven, Jr., J. A. Montgomery, J. E. Peralta, F. Ogliaro, M. Bearpark, J. J. Heyd, E. Brothers, K. N. Kudin, V. N. Staroverov, R. Kobayashi, J. Normand, K. Raghavachari, A. Rendell, J. C. Burant, S. S. Iyengar, J. Tomasi, M. Cossi, N. Rega, J. M. Millam, M. Klene, J. E. Knox, J. B. Cross, V. Bakken, C. Adamo, J. Jaramillo, R. Gomperts, R. E. Stratmann, O. Yazyev, A. J. Austin, R. Cammi, C. Pomelli, J. W. Ochterski, R. L. Martin, K. Morokuma, V. G. Zakrzewski, G. A. Voth, P. Salvador, J. J. Dannenberg, S. Dapprich, A. D. Daniels, Ö. Farkas, J. B. Foresman, J. V. Ortiz, J. Cioslowski and D. J. Fox, Gaussian, Inc., Wallingford CT, 2009.

- 12 O. V. Sizova, L. V. Skripnikov, A. Y. Sokolov and *J. Mol. Struct.: THEOCHEM*, 2008, **870**, 1–9.
- 13 A. E. Reed, L. A. Curtiss and F. Weinhold, *Chem. Rev.*, 1988, **88**, 899–926.
- 14 K. B. Wiberg, *Tetrahedron*, 1968, **24**, 1083–1096.
- 15 Z. Chen, C. S. Wannere, C. Corminboeuf, R. Puchta and P. v. R. Schleyer, *Chem. Rev.*, 2005, **105**, 3842–3888.
- 16 G. Schreckenbach and T. Ziegler, *J. Chem. Phys.*, 1995, **99**, 606–611.
- 17 M. Krykunov, T. Ziegler and E. v. Lenthe, *Int. J. Quantum Chem.*, 2009, **109**, 1676–168318
S. K. Wolff and T. Ziegler, *J. Chem. Phys.*, 1998, 109, 895–905.
- 19 S. K. Wolff, T. Ziegler, E. v. Lenthe and E. J. Baerends, *J. Chem. Phys.*, 1999, **110**, 7689–7698.
- 20 M. Ma, A. Stasch and C. Jones, *Chem. – Eur. J.*, 2012, 18, 10669–10676.
- 21 Z. D. Brown, P. Vasko, J. C. Fettingner, H. M. Tuononen and P. P. Power, *J. Am. Chem. Soc.*, 2012, **134**, 4045–4048.
- 22 W. Uhl, U. Schütz, W. Hiller and M. Heckel, *Z. Anorg. Allg. Chem.*, 1995, **621**, 823–828.